Geophys. J. Int. (2007) **168,** 431–445 doi: 10.1111/j.1365-246X.2006.03167.x

Dilatancy controlled spatiotemporal slip evolution of a sealed fault with spatial variations of the pore pressure

G. Hillers[1]* and S. A. Miller[2]

[1]*Institute of Geophysics, ETH Zurich, Zurich, Switzerland*
[2]*Department of Geodynamics and Geophysics, Geology Institute, University of Bonn, Bonn, Germany*

Accepted 2006 July 28. Received 2006 June 22; in original form 2005 November 29

SUMMARY

A range of observations suggest the formation and maintenance of sealed and hence overpressured compartments in fluid-infiltrated fault zones. It is assumed that hydromechanical properties of regions with variable pore pressure states control the fault's stability and thus its characteristic response, that is, seismic or aseismic slip accumulation. We investigate in a systematic parameter space study the effects of spatial variations in pore pressure on spatiotemporal slip evolution along a hydraulically isolated fault plane. The 3-D continuum model is governed by rate-and-state friction and constitutive laws for porosity reduction. We show that the model response is sensitive to the degree of overpressurization and the efficiency of dilatant hardening mechanisms. Low pore pressures and small dilatancy effects result in unstable response types, whereas high pore pressures and large dilatant effects lead to stable and aseismic creep. Regions with an unstable response are shown to support most of the stresses accumulated during interseismic periods. Accelerated slip nucleates preferably in regions of low pore pressure. Statistical properties of model seismicity produce a wide range of event sizes for moderate and large earthquakes, in the case where dilatant mechanisms are inefficient. In case of efficient slip rate controlled porosity increase, less instabilities grow into large earthquakes. Final slip maps demonstrate the applicability of the chosen method to model seismicity controlled by frictional and hydraulic processes on a planar fault plane. The evolution of governing variables that depend on the pore pressure environment provide a conceptual basis for the interpretation of observed response characteristics.

Key words: complex slip evolution, dilatancy hardening, fluids and fault zones, rate-and-state friction.

1 INTRODUCTION

The presence of fluids in the Earth's crust and its mechanical effects on the seismogenic process is a well-documented but still not well-understood phenomenon because of feedbacks among several possible hydromechanical mechanisms that are difficult to separate. Numerous studies identified the potential importance of fluid migration following a main shock producing aftershock sequences (e.g. Nur & Booker 1972; Bosl & Nur 2002; Miller *et al.* 2004; Piombo *et al.* 2005, and references therein). Free fluids are expected to be involved in seismic swarm activity (Waite & Smith 2002), and they remotely triggered earthquakes in geothermal and volcanic areas (Husen *et al.* 2004). Stabilizing as well as weakening fluid-related mechanisms during rapid seismic slip, such as dilatant hardening and pore fluid expansion due to shear heating, respectively, are assumed to alter rupture propagation in large earthquakes (Garagash & Rudnicki 2003a,b). These competing mechanisms act on different time and velocity scales, that is, hardening effects influence nucleation phases associated with small slip rates, whereas thermal pressurization has a negligible effect during initial stages but becomes important when the sliding velocity is high (Andrews 2002). The dominating effect of thermohydraulical processes during seismic slip was shown to control the evolution of the friction coefficient and thus the rupture propagation in recent dynamic numerical experiments (Bizzarri & Cocco 2006a,b). The observed rapid slip-weakening behaviour substantially controls the imposed friction law which is necessary to model observed seismograms (Andrews 2006).

A number of laboratory and field observations confirm the formation and maintenance of low-permeability seals between the fault gouge and the host rock (Sibson 1994) that effectively trap pore fluids and lead to the formation of a conduit in the fault's core (Moore *et al.* 1994; Zhang & Tullis 1998; Zhang *et al.* 1999, 2001). Porosity reducing mechanisms that can lead to overpressured fluid states are

*Now at: Institute for Crustal Studies, University of California, Santa Barbara, USA. E-mail: gregor@crustal.ucsb.edu

plastic pore closure, stress-induced dissolution and crack healing and sealing (Walder & Nur 1984; Nur & Walder 1992; Sleep & Blanpied 1992; Blanpied *et al.* 1998; Lockner & Byerlee 1994). Alternatively, near-lithostatic fluid regimes can result from continued upwelling of overpressured fluids from the bottom of the seismogenic part of the crust (e.g. Rice 1992), or dehydration of hydrous minerals from frictional heating. Hydraulically isolated overpressured fault zones remain sealed indefinitely even though occasional fault valve behaviour (Sibson 1992; Cox 1995)—breaking the seals during large slip events—may temporarily allow the equilibration of pore pressure states in-and outside the fault zone (Blanpied *et al.* 1992).

The San Andreas fault's strength is found to be anomalously low, based on the lack of a significant aberrant heat flow signal accompanied by borehole stress measurements indicating a steep angle between the fault's strike and the maximum compressive stress (Lachenbruch & Sass 1980; Hickman 1991). An explanation that satisfies both constraints are elevated pore pressures reducing sufficiently the frictional strength (Rice 1992). Heterogeneous fault zone materials with different physical properties exposed to pore compacting mechanisms is a likely cause of different degrees of overpressurization in a fault zone. Focusing on this mechanism Lockner & Byerlee (1995) conducted a numerical study of a 1-D Burridge–Knopoff type model (Burridge & Knopoff 1967), where most of the shear stress is supported by a small number of compartments with relatively low pore pressure. Miller *et al.* (1996) extended this concept to a 2-D fault plane with a simple model for fluid pressure variation within the fault zone. In this study we adopt these concepts (Fig. 1) and investigate, in a systematic parameter space study of a 3-D continuous fault model, the effect of variable fluid pressures trapped in a sealed fault zone on spatiotemporal slip evolution.

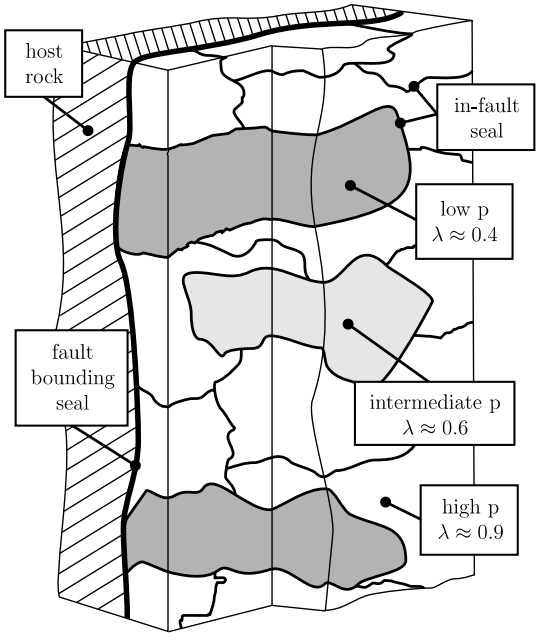

Figure 1. Conceptual model. Cut-away schematic view after Lockner & Byerlee (1995). A hydraulically isolated fault core develops compartments with different degrees of overpressurization, ranging from near-hydrostatic ($\lambda \approx 0.4$) to near-lithostatic ($\lambda \approx 0.9$) conditions. Assuming heterogeneous material properties, pore space compacting mechanisms lead to the formation and maintenance of these pockets. For simplicity, we neglect temporal evolution of in-fault seals, prohibiting the equilibration of different pore pressure states inside the fault's core.

Previous 3-D hydromechanical strike-slip fault models investigated the properties of spatiotemporal seismicity controlled by fluid-related mechanisms, such as the development of sealed pockets of high pore pressure and permeability changes during the seismic cycle (Miller *et al.* 1996, 1999; Fitzenz & Miller 2001). These models demonstrated the simplicity of generating and maintaining complexity along a fluid-infiltrated fault zone by including dominant hydromechanical effects. Their inherent discreteness, however, led to generic results such as slip events with physically plausible properties that make it difficult to estimate the relative importance of fluid-related processes, since purely elastic models of the discrete class have been shown to generate complex slip evolution and seismicity over a wide range of sizes without fluid interaction (e.g. Burridge & Knopoff 1967; Langer *et al.* 1996; Carlson & Langer 1989a,b; Carlson *et al.* 1991; Bak *et al.* 1987, 1988; Bak & Tang 1989; Ito & Matsuzaki 1990; Lomnitz-Adler 1993; Ben-Zion 1996; Zöller *et al.* 2005a,b; Dahmen *et al.* 1998). The quasi-dynamic continuous approach presented in this study aims to investigate qualitatively the nucleation, propagation and arrest of slip instabilities in a sealed, and thus overpressured, fluid-infiltrated fault in a consistent framework. The modelling emphasis is the long-term slip evolution and different response characteristics of different regions on the fault, stable or unstable, which are controlled by pore pressure dependent hydromechanical interactions. Although the quasi-dynamic approach produces a solution of the coseismic evolution of the governing variables, we recognize that neglecting inertia, the normal stress dependence of the state variable, and temperature dependence may limit the accuracy of the details of the rupture process. Nevertheless, much can be learned about the interaction of hydromechanical effects and additional mechanism can be investigated in future studies.

We use the 3-D elastohydraulic model of Hillers & Miller (2006) who investigated the origin of slip complexity due to dilatancy as a function of permeability structures in the off-fault dimension using homogeneous properties along strike. The use of rate-and-state friction allows multicycle simulations, and results are compared to purely elastic models to extract the contribution of hydraulic parameters. The approach is an extension of a 1-D spring-block model discussed by Segall & Rice (1995) to study the efficiency of dilatant hardening mechanisms to suppress unstable sliding. Hillers & Miller (2006) showed that homogeneous frictional and hydraulic properties can lead to non-uniform, dilatancy controlled slip histories for a realistic range of parameters. In this paper, we expand this work by using heterogeneous distributions of variable pore pressure regimes along the fault, ranging from hydrostatic to near lithostatic, which have been shown to describe realistic properties of weak, mature fault zones. We show that it is important to model the physically probable spatial variations in pore pressure along strike with an appropriate 3-D model to study the interaction of different pore pressure regimes on a fault. Because of the dominant role of the spatial heterogeneity of overpressure on the fault's stability, the results are discussed in the context of complexity generating processes to identify the controlling mechanisms.

The remainder of the paper is organized as follows. In Section 2, we discuss the conceptual model and its implementation in the numerical model, followed by an introduction of basic parameter setting (Section 3). Section 4 describes spatiotemporal slip evolution as a function of the degree of overpressurization and dilatant mechanisms. We introduce a procedure to extract physical quantities from our simulations in Section 5, before we discuss

statistical properties and hypocentre locations of model seismicity in Sections 6 and 7, respectively. Finally, we focus on the temporal evolution of variables depending on the degree of overpressurization (Section 8).

2 MODEL

2.1 Conceptual model

We use a modified version of the conceptual model proposed and modified by Lockner & Byerlee (1995) and Miller *et al.* (1996), respectively, where isolated pockets with different degrees of overpressurization due to implicitly assumed material heterogeneities form in a fault's core which is hydraulically isolated from the host rock (Fig. 1). Intuitively, such along-strike variations will significantly influence rupture characteristics, and in this context we wish to quantify these effects. The concept matches the 'localized barriers' scheme from Caine *et al.* (1996), where a well-developed fault core situated in a poorly developed damage zone allows potential fluid flow. The degree of overpressurization is parametrized by

$$\lambda = \frac{p}{\sigma_n}, \tag{1}$$

with p, σ_n denoting the pore pressure in the fault zone and lithostatic normal stress, respectively. As has been discussed by Lockner & Byerlee (1995), low λ ($\equiv$ low p) regions are assumed to support most of the shear stress on the fault, since overpressured areas tend to slip in a stable manner. To investigate hydraulically controlled seismic response types on faults with heterogeneous λ distributions, we use the 3-D model of a fluid-infiltrated fault developed by Hillers & Miller (2006). This model expands the 1-D elastohydraulic model by Segall & Rice (1995) with the 3-D elastic approach of Rice (1993) to a fluid-infiltrated 2-D vertical strike-slip fault plane embedded in an infinite elastic half-space with rigidity $G = 30$ GPa, and shear wave velocity $v_s = 3\,\mathrm{km\ s^{-1}}$. The fault's response to continuous stressing induced by aseismic plate movement of $v^\infty = 35\,\mathrm{mm\ yr^{-1}}$ at $z < -24$ km is governed by rate- and state-dependent friction, dilatancy and pore compacting mechanisms (Fig. 2). Pore pressure regimes in- and outside the fault's core, p and p^∞, respectively, are modelled to equilibrate potentially over a length scale L_D, which scales the hydraulic diffusivity c to the effective diffusivity $c^* = c/L_D^2 = \kappa/(\nu\beta L_D^2)$ (Segall & Rice 1995).

Values of the permeability κ range from 10^{-19} m^2 to 10^{-14} m^2, even across a single fault line (Wibberly & Shimamoto 2003). Low permeabilities that lead to essentially undrained faults as considered here are on the order of 10^{-19} m^2, prohibiting effectively any fluid flow between the fault's core and the crustal bulk. The parameter $\beta = 5 \times 10^{-4}\ \mathrm{MPa^{-1}}$ is equal to the porosity, ϕ, times the sum of fluid- and elastic pore compressibility, respectively, and is assumed to be constant (Segall & Rice 1995), although the porosity is time dependent. The stability of the system is thus controlled by a constant effective hydraulic diffusivity, and by a slip rate induced pore compaction term discussed below. Likely interactions and feedback mechanisms of temperature changes, fault valve related fluid flow, crack formation in the off-fault dimension during rapid slip, and chemical cementation processes, which are usually difficult to separate, are not parametrized in this study. Assuming a viscosity of water at 60°C, $\nu \approx 5 \times 10^{-4}$ Pa s, and a thickness of the cemented border, L_D, of the order of 10 m (50 m) (Wibberly & Shimamoto 2003), c^* is of the order of $10^{-2}\ \mathrm{yr^{-1}}$ ($5 \times 10^{-4}\ \mathrm{yr^{-1}}$).

To isolate the effects of variable degrees of overpressurization we assume the hydraulic diffusivity, c^*, to be constant and homogeneous across the fault plane. The equilibration of p and p^∞ is restricted using undrained conditions ($c^* \to 0$) to account for sealed faults that develop spatially variable pore pressure regimes in their core, which can vary from hydrostatic ($\lambda \approx 0.35$) to near-lithostatic ($\lambda \approx 0.9$) conditions. We approximate heterogeneous pore pressure states by using 2-D λ distributions, and the pore pressure changes with respect to these initial conditions by slip rate controlled pore compaction. Hence, the degree of heterogeneity is quenched and its evolution and maintenance is not modelled explicitly by physical processes. Because the quasi-dynamic approach in tandem with heterogeneous hydraulic properties along the fault is shown to be limited in producing realistic coseismic slip rates, we follow Hillers & Miller (2006) interpreting intermittent accelerations as unstable, seismic slip events, even if the associated slip rates are much lower than natural velocities.

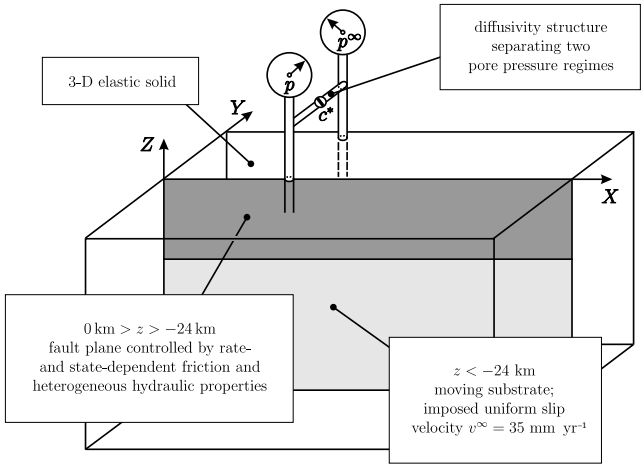

Figure 2. Corresponding numerical model of the conceptual model shown in Fig. 1: 2-D vertical strike-slip fault plane controlled by rate- and state-dependent friction, embedded in a 3-D elastic half-space, loaded by aseismic slip rate v^∞ at its downward extension. Variable pore pressure regimes in the fault, $p(x, z, t)$, are connected via effective hydraulic diffusivity, c^*, to the pore pressure state in the crustal bulk, $p^\infty(z)$. Slip is calculated over a depth range of 0 km $> z > -24$ km, where governing equations apply (dark grey area). The periodic repeat distance along strike is 100 km.

2.2 Modelling procedure

The 3-D model geometry and coordinate system (Fig. 2) used in this study are discussed in detail by Hillers & Miller (2006). We apply a boundary integral method where the spatiotemporal evolution of the governing variables are calculated on the fault plane (x, $y = 0$, z). Using the Dieterich–Ruina form of the friction coefficient's rate-and-state dependence,

$$\mu(x,z,t) = \mu_0 + a(z)\,\ln\left(\frac{v(x,z,t)}{v_0}\right) + b(z)\,\ln\left(\frac{v_0\,\theta(x,z,t)}{L}\right), \tag{2}$$

and assuming $\dot{p} \neq 0$, the temporal change of the state variable, θ, and the slip velocity, $v = \dot{u}$, is (Segall & Rice 1995)

$$\frac{\partial\theta(x,z,t)}{\partial t} = 1 - \frac{v(x,z,t)\,\theta(x,z,t)}{L(x,z)}$$

$$\frac{\partial v(x,z,t)}{\partial t} = \left(\frac{\dot{\tau}^r(x,z,t) + \mu(x,z,t)\,\dot{p}(x,z,t)}{\sigma_e(x,z,t)} - \frac{b(z)\,\dot{\theta}(x,z,t)}{\theta(x,z,t)}\right) \times \left(\frac{\eta}{\sigma_e(x,z,t)} + \frac{a(z)}{v(x,z,t)}\right)^{-1}. \tag{3}$$

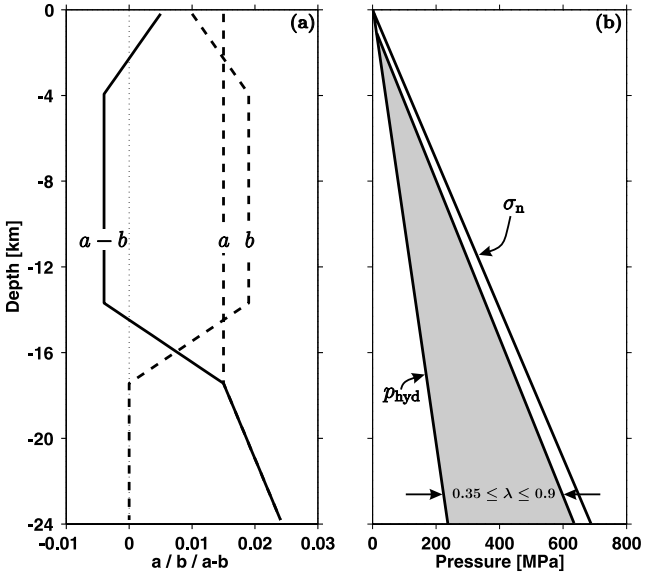

Figure 3. (a) Applied a, b and $a - b$ profile. (b) Lithostatic normal stress, σ_n, and hydrostatic pore pressure, p_{hyd}. The grey area denotes physically probable overpressured pore fluid states, bounded by $\lambda = p/\sigma_n = 0.35$ and $\lambda = 0.9$ (Miller *et al.* 1996, 1999).

Here, the state variable evolves according to the 'slowness' or 'aging' form of the friction law, and L is a characteristic length scale over which a new population of contacts between two surfaces evolves, depending on fault roughness and gouge width (e.g. Marone 1998; Ohnaka 2003, and references therein). The empirical parameters a and b relate changes in slip rate and state to frictional strength (Fig. 3a), and μ_0 and v_0 are normalizing constants (Rice *et al.* 2001). In eq. (3) the evolution of the slip velocity depends on the time derivative of

$$\tau_{ij}^{r}(t) = \sum_{k=1}^{nx} \sum_{l=1}^{nz} K_{|i-k|,j,l} \left(v^{\infty} t - u_{kl}(t)\right), \tag{4}$$

the convolution of the slip deficit field with the elastostatic kernel or Green's functions matrix K (for indexing see Hillers *et al.* 2006a), leading to $\dot{\tau}^{r} \propto (v^{\infty} - v)$. The effective normal stress is denoted by $\sigma_e(x, z, t) = \sigma_n(z) - p(x, z, t)$. Seismic radiation damping is approximated by $\eta = G/2v_s$ (Rice 1993). The shear stress on the fault is computed using

$$\tau_{ij}(t) = \tau^0 + \tau_{ij}^{r}(t) - v_{ij}(t)\,\eta, \tag{5}$$

with $\tau^0 = 100$ MPa (Hillers & Miller 2006). The quasi-dynamic description neglects inertia in eqs (3) and (5), that is, the stress changes that would result from an elastodynamic analysis are transmitted instantaneously (Taylor & Rice 1998). Linker & Dieterich (1992) observed a transient change of the shear resistance in normal stress stepping experiments, which is not explicitly parametrized in the present study because pure strike-slip motion does not alter the lithostatic normal stress component on the fault. However, changes in the effective normal stress (σ_e) and pore pressure changes ($\dot{p} \neq 0$) in eq. (3) control the slip rates and thus the evolution of the friction coefficient. That is, the effect of porosity controlled pore pressure changes is considered by $\dot{p} \neq 0$, but not parametrized by a normal stress dependence of the state variable.

Based on the derivation of Segall & Rice (1995) and its implementation to the present geometry by Hillers & Miller (2006), we use the simplified diffusion equation for the pore pressure evolution

$$\frac{\partial p(x, z, t)}{\partial t} = c^* \cdot (p^{\infty}(x, z) - p(x, z, t)) - \frac{\dot{\phi}(x, z, t)}{\beta}. \tag{6}$$

Here, the effect of temperature changes due to frictional heating on the pore pressure evolution is neglected. However, we can safely approximate constant temperature conditions in the present framework, since slip rates associated with large events at which these effects are dominant ($v > 0.1$ m s^{-1}, Bizzarri & Cocco 2006b) are not produced in our numerical experiments. This is because the spatial heterogeneity in the pore pressure states does not allow instabilities to grow into large events that develop realistic slip rates. A further but computationally necessary simplification is the static treatment of the pressure state inside the fault zone, that is, we do not calculate fluid flow in the $x - z$ plane of the fault, hence neglecting possible fault valve behaviour and its effects on seismogenesis. Eq. (6) shows that the temporal evolution of the pore pressure depends on the gradient of p and p^{∞} weighted by the effective diffusivity c^*, and on a plastic porosity reduction term proportional to $\dot{\phi}(x, z, t)$. In contrast to Hillers & Miller (2006), who used homogeneous c^* distributions to investigate the effect of drained ($c^* \to \infty$) and undrained ($c^* \to 0$) conditions, we apply diffusivities representing a hydraulically isolated fault core. With $c^* \to 0$, $\partial p/\partial t$ is effectively controlled by plastic porosity changes, $\dot{\phi} \neq 0$, the second term on the right hand side in eq. (6).

The constitutive law for porosity changes, $\dot{\phi}$, is based on laboratory experiments (Lockner & Byerlee 1994; Marone *et al.* 1990), which have been interpreted from the viewpoint of the steady state concept in soil mechanics (Segall & Rice 1995). Conceptually, a constant slip speed porosity evolves over the same length scale, L, as the state variable θ towards a steady state value

$$\phi_{ss} = \phi_0 + \varepsilon \ln\left(\frac{v(x, z, t)}{v_0}\right) \tag{7}$$

according to

$$\frac{\partial \phi(x, z, t)}{\partial t} = -\left(\phi(x, z, t) - \phi_{ss}\right) \frac{v(x, z, t)}{L}, \tag{8}$$

where ϕ_0 and ε denote a reference porosity and the dilatancy coefficient, respectively, parameterizing the efficiency of pore space increase due to accelerated slip. Sleep *et al.* (2000) found $\varepsilon \approx 3.4 \times 10^{-3}$ after long hold times, and Segall & Rice (1995) inferred $\varepsilon \approx 2 \times 10^{-4}$ interpreting data from Marone *et al.* (1990), which were obtained at rather high slip velocities. As discussed by Hillers & Miller (2006) 3-D simulations using this value do not generate large instabilities, but ε might be significantly smaller at lower and hence more realistic slip rates during the nucleation phase. Note that the equations for state and porosity evolution are not coupled, since at zero velocity $\dot{\theta} = 1$ but $\dot{\phi} = 0$.

We solve the resulting set of six first-order ordinary differential equations in the variables $\dot{\mu}$, $\dot{\theta}$, $\dot{v}$, $\dot{p}$, $\dot{\phi}$, $\dot{u}$ using an implicit Runge–Kutta method for stiff systems with adaptive step-size control, RADAU5 (Hairer & Wanner 1996). We use the fast Fourier transform (FFT) to compute the convolution of the Green's functions matrix K with the velocity field, $v^{\infty} - v$ (Rice 1993; Stuart & Tullis 1995; Rice & Ben-Zion 1996). The model faults are 100 km long and 24 km deep, and discretized into 512×128 numerical cells along strike and depth, respectively. Details of the numerical procedure and specific solver parameters can be found in the appendix of Hillers (2006).

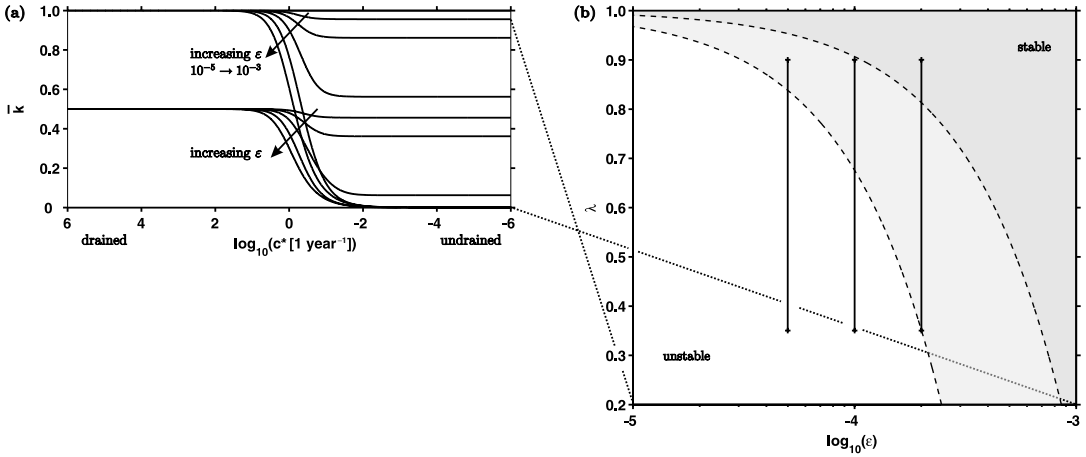

Figure 4. Different horizons of the multidimensional phase space. (a) Illustration of eq. (24) in Segall & Rice (1995), (normalized) critical stiffness, $\bar{k}$, as a function of effective diffusivity, c^*. The two line sets belong to a specific choice of frictional parameters a, b, and represent increasing values of the dilatancy coefficient, $\varepsilon = [10^{-5}, 5 \times 10^{-5}, 10^{-4}, 5 \times 10^{-4}, 10^{-3}]$. (b) Illustration of eq. (16) in Hillers & Miller (2006a), the degree of overpressurization, λ, as a function of the dilatancy coefficient, ε. The light grey region between stippled lines marks a transition zone between stable and unstable regions for a specific choice of $a - b = const$. Vertical lines represent the parametrization of models shown in Fig. 5. For a detailed analysis see Hillers & Miller (2006a).

3 PARAMETER SETTING

3.1 Critical nucleation size

For the current approach the condition $h \ll h^*_{\mathrm{u}}$ has to be met to solve the governing equations in the continuum limit (Rice 1993). That is, the spatial discretization of the numerical grid, h, has to be (much) smaller than the critical cell size for undrained conditions (Taylor & Rice 1998)

$$h^*_{\mathrm{TR}} = 2GL\left[\pi\left(\sigma_{\mathrm{e}}(b-a)_{\max} - \frac{\varepsilon\mu_0}{\beta}\right)\right]^{-1}. \tag{9}$$

Since we use spatially variable distributions of λ, the maximum value of the term in parenthesis is not only controlled by the depth-dependent $b - a$ distribution but also by maximum σ_{e} on the fault. As discussed by Hillers *et al.* (2006a) we do not claim our results are completely independent of the spatial resolution as in Lapusta *et al.* (2000). However, with $L = 0.05$ m used throughout this study we find that h/h^*_{TR} is always smaller than 0.2, which was found to be a healthy ratio satisfying the required $h \ll h^*_{\mathrm{TR}}$. We adopt initial conditions for p and p^∞ used by Hillers & Miller (2006). Since we parametrize sealed fault walls by setting $c^* \to 0$, the pore pressure evolution (eq. 6) is controlled almost exclusively by porosity changes (eq. 8). However, we use a small but non-zero value for c^*, and because we aim to avoid a continuously decreasing $h^*_{\mathrm{TR}} \propto 1/p$ in case p^∞ is hydrostatic (i.e. $p \gg p^\infty$), we use

$$p(x, z, 0) = p^\infty(x, z) = \max\left[p_{\mathrm{hyd}}(z), \sigma_{\mathrm{n}}(z) \cdot \lambda(x, z)\right]. \tag{10}$$

This treatment leads to hydrostatic conditions in the topmost part of the fault. Certainly, h^*_{TR} depends on changes in ϕ, but these changes are minor depending on ε (figs 4, 5, 10, 11 in Hillers & Miller 2006) and do not control the model's response because of time-dependent critical cell sizes. We create simple heterogeneous 2-D λ distributions to approximate different degrees of overpressurization, because the pore compacting mechanism (eq. 8) appears to be limited at generating and maintaining high fluid pressure (Segall & Rice 1995). Eq. (10) seems to overstretch hydraulically plausible conditions in the host rock, but we claim that this particular parametrization is necessary to control the fault's response only by spatial changes in λ across the fault. Setting $c^* = 0$ results in the same effect without taking p^∞ into consideration as in the conceptual model.

3.2 Stability regimes

Small diffusivities ($c^* \to 0$) approximate sufficiently undrained conditions, such that systems investigated in this study are located in the right part of the phase diagram displayed in Fig. 4(a). The figure shows the dependence of the critical stiffness normalized by its value in the drained limit,

$$\bar{k} = \bar{k}\,(L, \sigma_{\mathrm{e}}, a, b, \varepsilon, \mu_0, \beta, F(c^*)) \tag{11}$$

(eq. 24 in Segall & Rice 1995), where $F(c^*)$ varies non-linearly between 0 and 1. Since $k > \bar{k}$ and $k < \bar{k}$ results in stable and unstable responses of a rate-and-state controlled 1-D spring-block model (e.g. Ruina 1983), respectively, the relative location of a systems' actual stiffness, k, in the parameter space indicate whether stable creep or repeated slip instabilities develop in response to external loading (Hillers & Miller 2006). In the drained limit, stick-slip is the only possible response type since k is always smaller than $\bar{k}$ for $a < b$ at seismogenic depths (Fig. 2a). In the undrained limit, however, dilatant processes can stabilize an otherwise unstable fault if $1 > \bar{k} > k$ depending on ε, in particular on the size of $\varepsilon\mu_0/\beta$ relative to $\sigma_{\mathrm{e}}(b - a)$ (eq. 9). This shows that the consideration of hydromechanical processes in the rate-and-state framework expands the possible response regimes of a purely elastic system. Because the homogeneous $a < b$ distribution along strike at -3 km $< z <$ -15 km allow system-wide instabilities to occur (Tse & Rice 1986; Rice 1993; Lapusta *et al.* 2000), the generated non-uniform slip evolutions discussed here clearly result from heterogeneous hydraulic properties along the fault. For a complete discussion of the phase diagram, its implications and drained model responses see Segall & Rice (1995) and Hillers & Miller (2006).

Fig. 4(b) shows an alternative horizon of the multidimensional phase space, $\lambda = \lambda(\varepsilon)$ (eq. 16 in Hillers & Miller 2006). A relatively large value of $\varepsilon > 10^{-4}$ stabilize the system's slip evolution, whereas smaller ε values representing less-effective dilatant mechanisms leave the unstable stick-slip response unaffected. Since we use heterogeneous 2-D λ distributions with $\lambda \in [0.35\ 0.9]$ in tandem

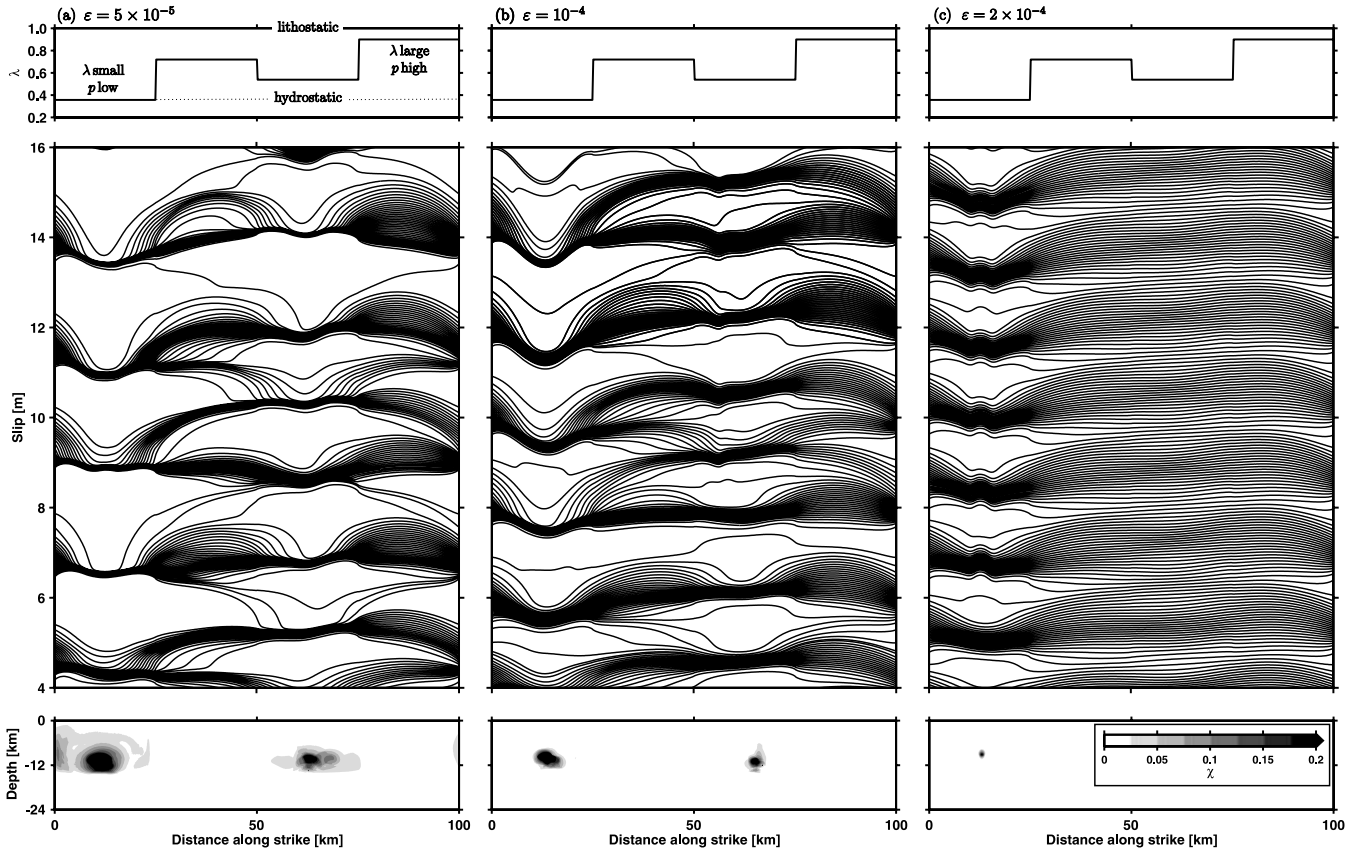

Figure 5. Slip histories controlled by heterogeneous 2-D λ distributions and dilatant mechanisms of variable efficiency. (a)–(c) The models share the same parameter set, except the dilatancy coefficient (Fig. 4b). Top row: Along-strike horizon of λ. Middle panel: Corresponding slip evolutions. Lines are drawn every two years. Bottom row: Resulting seismic coupling coefficient, χ.

with variable values of ε across the undrained fault, we anticipate different response characteristics of patches with different degrees of overpressurization (Hillers & Miller 2006). This shows that results depend not only on λ but also on $\varepsilon\mu_0/\beta$, because this ratio of competing mechanisms of dilatancy and compressibility of the pore space controls the stability of overpressured compartments (Taylor & Rice 1998; Hillers & Miller 2006). That is, Segall & Rice (1995) showed that $\varepsilon/\beta(b-a)$, weighted by the steady state friction coefficient, is the smallest value of σ_e for instabilities to develop. Unstable slip occurs only if a sufficient increase of the available pore space, ϕ, outperforms incompressibility, leading to a drop in pore pressure. Since $\mu_0 = 0.7$ and $\beta = 5 \times 10^{-4}$ MPa^{-1} are constant throughout this study, we discuss slip evolutions in terms of the parameter ε.

4 PORE PRESSURE AND DILATANCY CONTROLLED SLIP EVOLUTION

In a first set of simulations we approximate isolated fluid compartments by four square, equally sized patches along strike having different degrees of overpressurization. We divide the interval $[\lambda_{\min}, \lambda_{\max}] = [0.35,\ 0.9]$ equally into four (in later sections into 8×2 and 16×4) values and randomly assign one λ value from the interval to each cell of a certain patch (Hillers *et al.* 2006a). A horizontal cross-section of this λ distribution is shown in the top row of Figs 5(a)–(c). Each of the three models consists of the same set of parameters, except the dilatancy coefficient ε. The smaller ε, that is, the less effective the porosity increases, the more unstable the fault responses, leading to an inverse scaling between spatial seismic coupling,

$$\chi(x,z,t) = \frac{u(x,z,t)_{\text{seismic}}}{u(x,z,t)_{\text{total}}}, \tag{12}$$

and the dilatancy coefficient. This result is explained by the system's location in the $\lambda = \lambda(\varepsilon)$ plane where smaller values of ε are associated with more unstable conditions (Fig. 4b). Hillers & Miller (2006) showed that a less-effective increase of the pore space ($\dot{p} \approx 0$) leads to cyclic system-wide events, and that models with a larger degree of overpressurization show larger coseismic slip than corresponding low-λ simulations because of the relative weakness of the latter. This finding corresponds to the results shown in Fig. 5 suggesting a positive correlation between relatively small λ values and the nucleation and growth of instabilities. This relation is obvious for all three values of ε used but most significant for $\varepsilon = 5 \times 10^{-5}$. This trend can be understood by the position of the ε value on the abscissa axis in Fig. 4(b) with respect to the regions indicating stable or unstable response characteristics. Clearly, regions with low degrees of overpressurization develop the largest instabilities, that is, regions of low pore pressure show most seismic slip. It is important to note that the exclusive development of instabilities in low-p regions, and the correlation of low-p states with high-u_{seismic} regions is a fundamental outcome of the current approach. The explanation has been given by the 1-D stability analysis discussed above (Segall & Rice 1995). Comparing the spatiotemporal slip evolution of Fig. 5 to previously published work (e.g. Tse & Rice 1986; Rice 1993; Lapusta *et al.* 2000), the dominating effect of hydromechanical processes

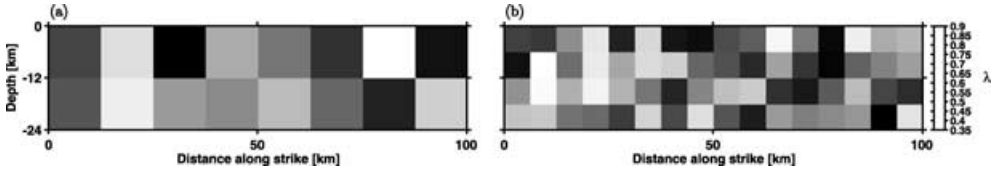

Figure 6. Two representative examples of heterogeneous 2-D λ distributions with (a) 8 × 2, (b) 16 × 4 patches along strike and depth, respectively.

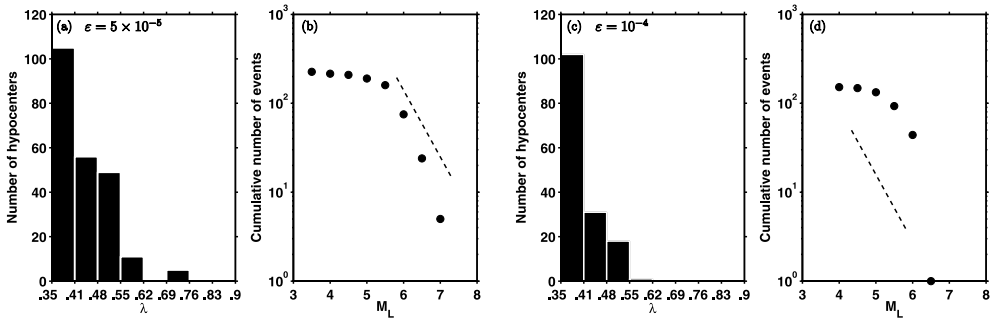

Figure 7. (a), (c) Number of hypocentre as a function of λ at the hypocentre, and (b), (d) corresponding FMD. The results are stacked from a number of simulations using several maps as in Fig. 6 with (a), (b) $\varepsilon = 5 \times 10^{-5}$, and (c), (d) $\varepsilon = 10^{-4}$. Stippled line in the FMD plots indicate a reference slope of the Gutenberg-Richter (GR) law characterizing seismicity pattern of global strike-slip events shallower than 50 km (Frohlich & Davis 1993).

becomes obvious, because homogeneous frictional properties, as applied in the present case, lead to repeated instabilities that rupture the entire fault in these purely elastic studies.

In terms of the Lockner & Byerlee (1995) concept (Fig. 1), regions with low pore pressures, supporting most of the fault's stress in interevent times, fail developing accelerated slip rates. The slip event is terminated in neighboured regions of high-p values, because there unstable slip cannot occur because of effective dilatant hardening mechanisms. We observe a time delay between slip events at lower-p regions (Fig. 5a, $x = [12,\ 63]$ km), with interceding creep in adjacent high-p regions. However, this pattern is not regular because sometimes the stable patch at $x = 12$ km slips prior to the one located at $x = 63$ km (e.g. $u = 5$–7 m), whereas in later sequences this patch becomes unstable first (e.g. $u = 14$–16 m). It is evident that heterogeneous λ distributions produce a persistent pattern of earthquake nucleation and variability in slip evolution that corresponds to the associated degree of overpressurization. Similar to Hillers *et al.* (2006a), where earthquakes nucleate in regions of low L values, the creeping and locked parts in the present simulations depend linearly on the dominating degree of overpressurization. This is in contrast to Liu & Rice (2005), where small variations in the frictional parameters a and $a - b$ along strike lead to non-linear and hence unpredictable slip pattern, and to Hillers & Miller (2006), where dilatant effects on a homogeneously parametrized fault produce non-stationary slip patterns.

Implicitly assumed seals bounding neighbouring patches against each other might break during seismic slip episodes and lead to equilibrated pore pressure regimes within the fault zone (Miller *et al.* 1996). These boundaries possibly reseal in interseismic periods and different degrees of compacting mechanisms or direct fluid sources at depth are assumed to lead to different degrees of overpressurization prior to the next slip event. Hence, a more realistic treatment of these mechanism known as 'fault valve behaviour' (Sibson 1992; Cox 1995) might add further degrees of complexity to seismicity evolution, as well as the explicit modelling of the influence of off-fault damage, shear heating, and chemical alteration of the material's properties.

5 EARTHQUAKE PARAMETERS

We generate seven different 2-D λ distributions with different degrees of heterogeneity, using 4 × 1, 8 × 2 and 16 × 4 patches along strike and depth, respectively (Fig. 6). To compare seismicity generated by this set of simulations we determine quantities that are listed in typical earthquake catalogues. We extract a seismic catalogue from the continuously simulated slip velocities generated by our numerical experiments using criteria for a seismic event introduced by Hillers *et al.* (2006a). The algorithm measures the cumulative slip of a compact zone of cells as long as its slip rates are larger than a certain velocity threshold, separating seismic from aseismic slip. For details on the definition and interpretation of stable, aseismic response in contrast to unstable, accelerated slip in the present quasi-dynamic framework with limited spatial and temporal resolution see Hillers & Miller (2006). The event size is measured by the scalar potency P (sum of seismic slip times rupture area in [km^2 cm]) (Ben-Zion 2003), and the corresponding event magnitude is obtained by an empirical scaling relation of Ben-Zion & Zhu (2002) for events larger than $M_{\mathrm{L}} = 3.5$, $\log_{10}(P) = 1.34\, M_{\mathrm{L}} - 5.22$. Hypocentres are identified as the cell whose sliding velocity first exceeds the threshold slip rate at the onset of slip instability.

6 STATISTICAL PROPERTIES

6.1 Frequency–magnitude distribution (FMD)

We perform two simulations for each of the seven λ distributions with $\varepsilon = 5 \times 10^{-5}$ and $\varepsilon = 10^{-4}$, respectively. We stack the resulting catalogues extracted with the procedure explained in Section 5 and plot the number of hypocentres as a function of λ at the hypocentre location and the FMD (Fig. 7). The histograms show that earthquakes nucleate preferably in regions where λ is low. Differences between Figs 7(a) and (c) reveal that the localization of hypocentres at low λ is more pronounced for larger ε, which has already been implied by Fig. 5. The FMDs confirm the trend that

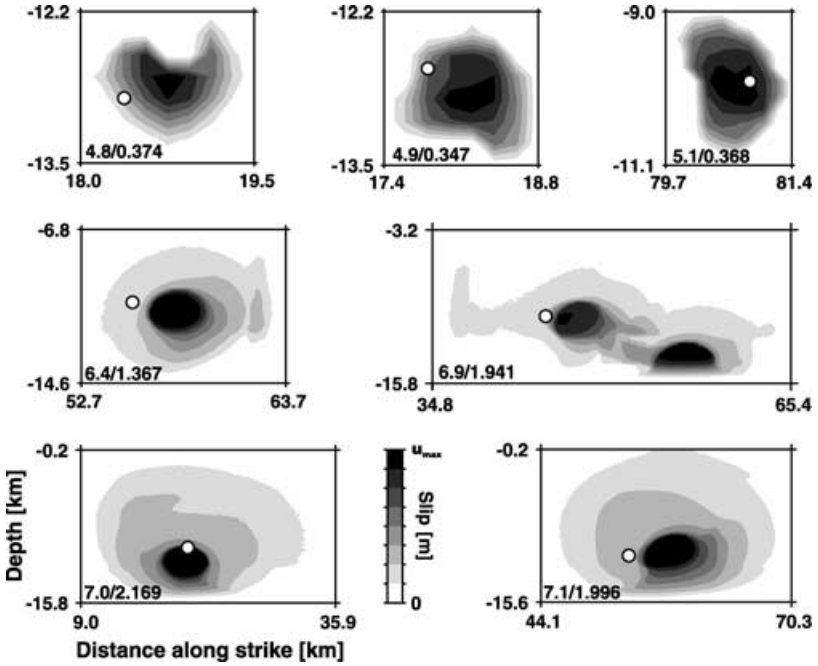

Figure 8. Examples of final slip distributions. Events from four different magnitudes ranges are taken from simulations corresponding to λ distributions shown in Fig. 6(a) and (b). Magnitude, M_L, and maximum slip, u_{max} [m], is given in the lower left corner of each slip map. Grey-intensity is scaled to u_{max} of each single event. White dots denote hypocentres. Given distances along strike and depth correspond to the actual position on the 100 km × 24 km fault.

different values of ε produce in general the same behaviour, but results differ in detail. If dilatant effects are relatively small we observe a clear break in scaling at $M_L = 5.5$. For larger magnitudes, the slope is comparable to the reference slope of a frequency size statistics characterizing global strike-slip events shallower than 50 km (Frohlich & Davis 1993). Earthquakes with magnitudes smaller than $M_L = 5.5$ occur far less often than an extrapolation of the slope to small magnitudes would imply. Thus, heterogeneous p distributions are sufficient to produce realistic FMD statistics only for moderate and large earthquakes.

Small slip events with magnitudes $M_L < 5$ are produced less frequently compared to continuous elastic models with heterogeneous distributions of the critical slip distance L (Hillers *et al.* 2006a,b), and to discrete models parametrizing structural heterogeneity (Ben-Zion 1996; Ben-Zion *et al.* 2003; Zöller *et al.* 2005a,b). This is partly due to the relatively large value of L used in the present study, which is an order of magnitude larger than in Hillers *et al.* (2006a) and Lapusta *et al.* (2000), resulting in an increased nucleation zone. Future studies using smaller L values are expected to generate seismicity with more realistic statistical properties over the entire magnitude range. Moreover, the linear range of λ is physically limited, compared to the logarithmic range of L in Hillers *et al.* (2006a) and Hillers *et al.* (2006b), indicating that the range of size scales is an effective tuning parameter (Ben-Zion 1996; Zöller *et al.* 2005b). For $\varepsilon = 10^{-4}$, the break in scaling in the FMD is less pronounced but shows a more gentle curvature of the FMD. It appears that only one $M_L \geq 6.5$ event in the whole set of simulations occurred, revealing the ability of increased dilatancy mechanisms to stabilize fault slip more effectively (Fig. 5c; Segall & Rice 1995; Taylor & Rice 1998; Hillers & Miller 2006).

Note that the overall productivity of the present implementation cannot be compared to the generation of model seismicity from previous 3-D discrete elastic (e.g. Ben-Zion 1996; Zöller *et al.* 2005b) and elastohydraulic models (e.g. Miller *et al.* 1999; Fitzenz & Miller 2001), and continuous elastic models with heterogeneous frictional properties (Hillers *et al.* 2006a,b). This is partly due to the numerically challenging implicit integration scheme, where the chosen spatial discretization of 512 × 128 cells along-strike and downdip allows the calculation of the solution only for a limited time interval. Furthermore, the present tuning parameter λ is relatively inefficient to produce seismicity with statistical properties similar to natural seismicity, compared to the effect of strong geometrical heterogeneities studied by Ben-Zion *et al.* (2003), Zöller *et al.* (2005b) and Hillers *et al.* (2006a).

6.2 Synthetic slip maps

We show a set of final slip maps (Fig. 8) generated by our quasi-dynamic simulations using pore pressure regimes with different degrees of heterogeneity across a fault. The slip distributions of specific events show the same characteristics as those generated by the rate-and-state friction model with spatial variations of the critical slip distance, although they lack some of the persistent second-order features such as multiple high slip areas (Hillers *et al.* 2006a). This proves that non-uniform pore pressure distribution on a fault are capable of producing heterogeneous slip maps of dynamic instabilities with properties comparable to examples of real ($M_L > 6$) earthquakes (Mai 2004). However, modelled quasi-dynamic coseismic slip ($u_{max} \approx 2$ m for $M_L 7$) generally tends to underrepresent slip values observed in large events ($u_{max} > 5$ m, M_W 7.2 Landers earthquake). Note that synthetic coseismic slip is larger in case the entire fault slips unstable (Hillers & Miller 2006). The visual similarity suggests the applicability of the chosen approach to study hydraulic mechanisms responsible for observed features of natural seismicity. Slip maps generated in a previous hydromechanical study of a 2-D fluid-infiltrated fault (Miller 2002) are strongly influenced by the governing discrete character of the numerical implementation

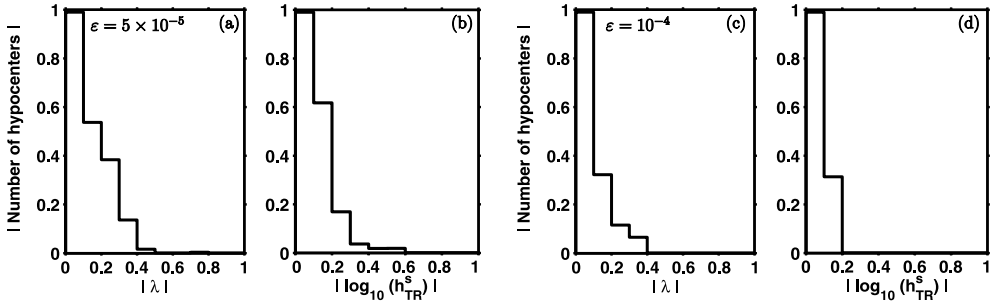

Figure 9. Normalized (to the maximum occurrence) number of hypocentres as a function of (a), (c) λ, and of (b), (d) the effective nucleation size, depending on the dilatancy coefficient, ε. The correlations show a maximum occurrence at small values, followed by an approximate 1/variable decay, similar to results found by Hillers *et al.* (2006a,b).

and the binary static/dynamic treatment of the frictional resistance, whereas in the present model the numerical grid does not control the solution. Hence, slip maps presented here are direct consequences of the interaction between regions of different degrees of overpressurization.

7 HYPOCENTRE LOCATIONS

7.1 Testing procedure

Following Hillers *et al.* (2006b) we test hypocentre locations (*HL*) generated by various simulations against 2-D distributions of physical parameters prevailing at the *HL* to investigate the dependence of earthquake nucleation on spatially varying hydromechanical properties of the fault zone. First we compare the *HL* to the original 2-D λ distribution, normalized by the underlying distribution of λ values. The second parameter is the effective nucleation size, $h^{\mathrm{s}}_{\mathrm{TR}}$, based on the estimate of Taylor & Rice (1998), $h^{\mathrm{n}}_{\mathrm{TR}}$, which is derived using eq. (9) with $\sigma_{\mathrm{e}}(x, z)$, $a(z)$ and $b(z)$. See Hillers *et al.* (2006b) for the derivation of h^{s}. Parameters are normalized to the range [0 1] to be comparable among each other.

7.2 Hypocentre locations

Fig. 9 displays the normalized histograms of hypocentre locations as a function of normalized parameter range of λ and $h^{\mathrm{s}}_{\mathrm{TR}}$. Clearly, most slip instabilities nucleate in regions where λ and hence the pore pressure is low, as outlined in Fig. 7. For both model classes with $\varepsilon = 5 \times 10^{-5}$ and $\varepsilon = 10^{-4}$, respectively, the maximum occurrence of *HL* can be found at smallest values, followed by an approximate $1/\lambda$ decay toward larger values. The same behaviour is observed by Hillers *et al.* (2006a) and Hillers *et al.* (2006b) in a number of models, where most earthquakes tend to nucleate in regions where the heterogeneity parameter L is small, followed by a similar decay. Hence, both models produce most earthquakes in regions that are most likely to become unstable because of smallest nucleation sizes. This is confirmed in the correlation of *HL* with $h^{\mathrm{s}}_{\mathrm{TR}}$, showing a pronounced localization at small values. Within the framework of the present study, and assuming the present ε values to be realistic, these observations imply that stress sustaining portions during interseismic periods can be interpreted with regions having a low pore pressure state that have the tendency to develop intermittent instabilities. Those low-p regions may be labelled strong, opposite to weak high-p regions. Note that this correspondence is justified in the framework of the present model implementation. In terms of the present nomenclature Rice (1993), Rice & Ben-Zion (1996), Lapusta *et al.* (2000) and Hillers *et al.* (2006a) used an effective normal stress at seismogenic depth of $\sigma_{\mathrm{e}} = 50$ MPa, leading to a rather high λ and thus weak fault zone. Ben-Zion & Rice (1995) used heterogeneous but static pore pressure profiles to explore its effects on slip evolution. However, because these elastic models do not explicitly simulate the evolution of the pore space and associated pore pressure changes, and its effect on fault zone stability, an implication about the role of fluids cannot be deduced from their results.

A persistent observation in the present study is the negative correlation between earthquake nucleation and high pore pressures. However, the identification of high-p regions as weak zones seems to imply just the opposite. It is important to note that the weak zones tend to release tectonic load by aseismic, steady stable sliding (Fig. 5c), whereas strong low-p zones fail seismically, developing intermittent instabilities. This response pattern is an original outcome of the present parametrization, leading to stable response modes due to effective dilatant mechanisms in the undrained limit. Possible rapid in-plane fluid flow that might trigger earthquakes due to a sudden drop of σ_{e} is not considered here.

8 EVOLUTION OF VARIABLES

We observe pore pressure controlled response functions along the fault. Fig. 10 shows stress and normalized velocity evolutions, $\tau = \tau(u)$ and $v = v(u)$, respectively, along a fault with a hydrostatic pore pressure regime. The model contains a high-p compartment deliberately placed slightly offset from the centre of the fault to investigate its effect on rupture spreading and the associated evolution of governing variables τ and v. Hydraulic barriers, that is, stably sliding overpressured regions, are imposed around $x = 0$ km (recall the use of periodic boundary conditions), such that the arrangement is intended to trigger instabilities around $x \approx 75$ km. However, the non-linearity of the system's response and its resulting slip evolution makes it difficult to trigger an event at a certain *a priori* specified place. In fact, very few instabilities emerge that develop a rupture front that passes the high-p patch at the fault's centre. Rupture speed and slip rates do not reach realistic values, hence the result is intended to illustrate qualitatively the effect of the overpressured patch. For example, slip velocity ranges only four orders of magnitude, whereas in fully dynamic treatments the difference in slip rates between locked and slipping episodes is as large as 10 orders of magnitude (Lapusta *et al.* 2000). The origin of the abscissa, $u = 0$ m, corresponds to the slip horizon at the beginning of the instability, which is not necessarily balanced along the fault (Fig. 5). During the course of the system's spatiotemporal evolution,

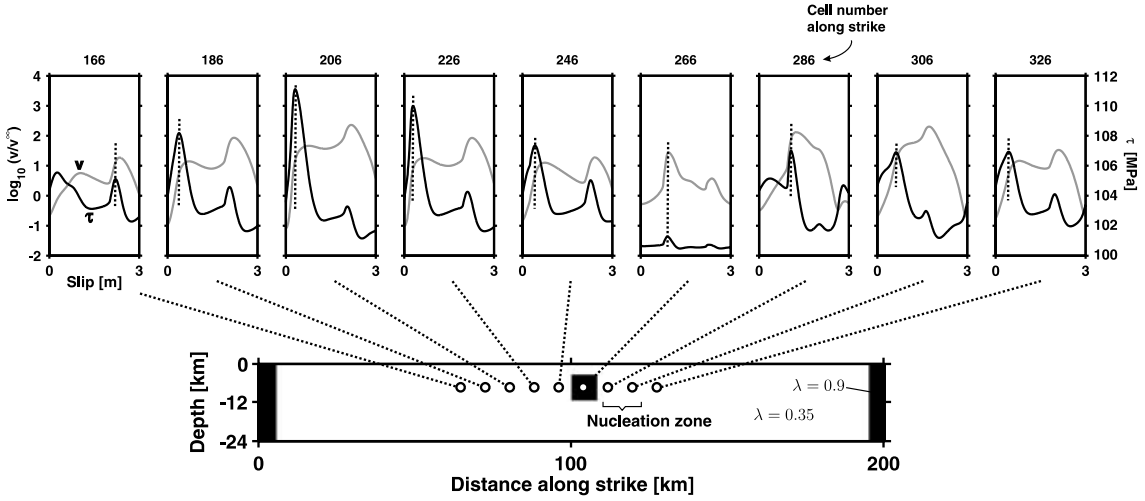

Figure 10. Temporal stress and associated velocity evolution, respectively, along a sealed fault with hydrostatic pore pressure. The imposed barrier centred at $x = 0$ km confines dynamic instabilities to the centre part of the fault plane. The patch at $x \approx 100$ km is placed deliberately to investigate its response and effect on passing rupture fronts. An instability nucleates at around cells 280–300, and the response functions for several locations on the fault are shown in the corresponding panels. The high-p patch (cell 266) shows a significantly different response character compared to adjacent regions where p is low. This is due to the patch's location in the stable portion of the parameter space. Slip $u = 0$ m refers to accumulated slip at the onset of the instability. $\varepsilon = 5 \times 10^{-5}$.

an instability nucleates around cells 280–310 where p is hydrostatic. The shape of the resulting velocity function (Fig. 10, cells 286, 306) show a gradual rise, and a distinct maximum before it drops to its interseismic regime. The corresponding stress curves reach their maximum prior to the maximum slip rates, and drop to the frictional sliding level, in agreement with kinematic and fully dynamic yet dry investigations (Tinti *et al.* 2004; Piatanesi *et al.* 2004).

At $x > 125$ km the instability soon dies out because of the stabilizing effect of the high-p patch centred at the model's origin. This behaviour might be a particular feature of the quasi-dynamic treatment where realistic slip rates of the order of a meter per second are not reached. A fully dynamic solution that considers heating effects is likely to produce different stopping mechanisms. We can isolate a relatively mature rupture front that passes the high-p patch left of the hypocentre. At the passage, the stress pulse remains significantly smaller compared to the surrounding low-p regions, since the compartment's response is stabilized by dilatant mechanisms and hence cannot support large shear stresses. The velocity, however, is of the same magnitude as the slip rates developed left of the patch. This indicates that the velocity evolution of the overpressured region does not differ qualitatively from the hydrostatic regions, but associated quasi-dynamic stress levels are significantly lower. At cells 186–246 the event produces prominent stress pulses. Here, too, the peak stresses are reached prior to the maximum slip rates, suggesting an initial slip hardening phase and a delayed initiation of dynamic fault weakening. Hence, acceleration is not accompanied instantaneously by weakening mechanisms, as suggested by Ohnaka (1996), Ohnaka & Shen (1999), and Ohnaka (2003). A similar observation has been made by Bizzarri *et al.* (2001) in a purely elastic drained model, suggesting this effect is not caused by the explicit consideration of dilatant mechanisms, but by the use of rate-and-state friction. Except in the nucleation zone and the high-p patch, the maximum slip rates—and corresponding stress pulses—are reached towards the end of the slip event, and are caused by reflected slip waves at the instability's boundaries. To the left of cell 186, the slip event ceases approaching the stable barrier. The overall complexity and heterogeneity of the curves among the observation points is a consequence of the evolutionary character of the current approach, different to the aseptic and stylized approach of simulations of a single dynamic rupture with homogeneous properties and forced nucleation. Therefore, details of the response functions like the relative position of curve peaks are due to the precise state of the system prior to the instability. Nevertheless, the clear difference between the responses of the high- and low-p regions is of general validity.

We extend the specific analysis of this tuned example and present response functions obtained at computational points at seismogenic depth for a typical example of a heterogeneous 2-D λ distribution that consists of 8×2 patches (Fig. 11). We plot responses from two locations in each λ patch, indicating that they essentially coincide but are nevertheless influenced by the response of adjacent patches (cells 80/112 and 336/368). The variable's histories display the evolution over several non-uniform cycles (Fig. 5), confirming that modelled coseismic slip (Fig. 8) is smaller than what is observed in real seismicity. Although limited in its resolution, this example serves as a conceptual basis for interpreting different response characteristics along a fault zone based on non-uniform hydraulic properties. The essence of this and other simulations (not shown) is that regions of low-p exhibit larger stress drops than regions of high-p, where exact results depend on specific choices of the dilatancy coefficient (Fig. 7). Small patches of high-p surrounded by larger areas of low-p show a significantly lower stress pulse when a rupture is passing (e.g. cell 400, see Fig. 10). From this bimodal (low/high-p) point of view, $\tau(u)$ functions shown in Fig. 11 give a broader overview over possible response types. The stress functions confirm the result by Lockner & Byerlee (1995) that areas of low-p have a higher stress level than neighbouring regions of high-p (e.g. cells 368, 400).

Corresponding slip rates reveal a dependence of maximum slip velocities on the degree of overpressurization. We find that patches with low λ develop slip rates that are up to two orders of magnitudes larger than regions with a large λ (e.g. cells 144, 400). However, the spatial λ heterogeneity connected to a relatively large cell size leads to slip rates of these high-p regions that are significantly larger than the background driving rate, v^{∞}. The particular response of overpressured regions is governed by the efficiency of dilatant

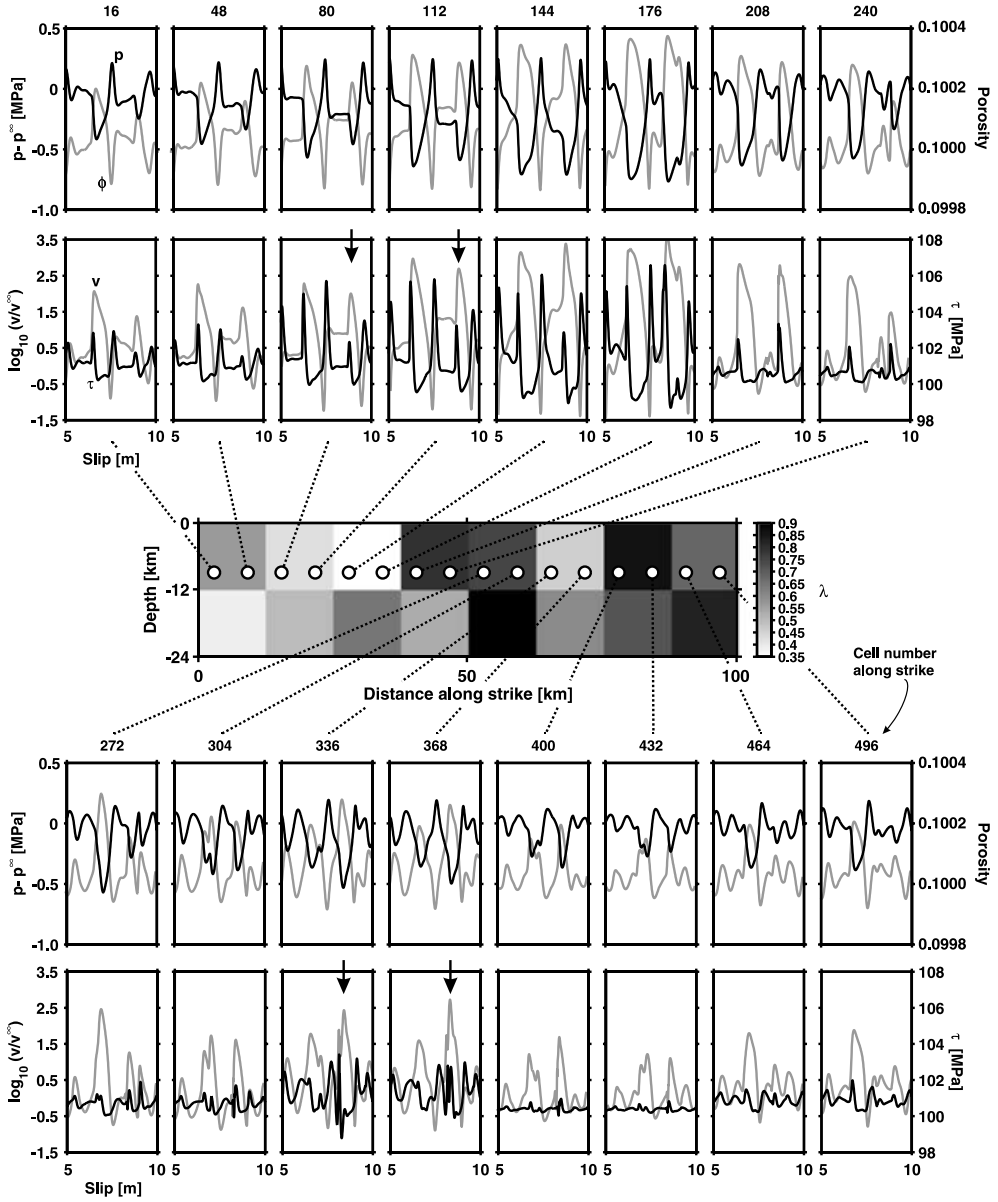

Figure 11. Response functions of a number of along-strike positions on a fault with heterogeneous 2-D λ distribution (middle panel). First, third row: Pore pressure ($p - p^{\infty}$, solid line) and porosity (ϕ, grey line) changes. Second, fourth row: Stress (τ, solid line) and normalized velocity ($\log_{10}(v/v^{\infty})$, grey line) changes. Porosity evolution shows the same character as the slip rate evolution. Pore pressure changes depend inversely on changes in porosity. Stress levels and stress changes of low λ regions are higher than in high λ regions, demonstrating that hydromechanical mechanisms control the strength of different areas along the fault. Arrows at cells 80/122, 336/368 highlight the influence on stress response from adjacent pressure states. $\varepsilon = 5 \times 10^{-5}$.

mechanisms, as demonstrated in Figs 5(a) and c, for example, at $x = 70$ km, where small values of ε allow $v \gg v^{\infty}$, but $v \approx v^{\infty}$ for ε being relatively large. That is, the continuum limit approach leads to accelerated slip rates of high-p regions if ε is sufficiently small, as these regions are passed by growing ruptures, which nucleate in low-p areas (Fig. 10). Hence, the modelling provides a physical explanation for slow slip events preceded and/or followed by seismic slip events (Segall 1996; Reilinger *et al.* 2000; Hearn & Reilinger 2002).

Porosity evolution illustrates the velocity dependence of ϕ (eq. 8), since $v(u)$ and $\phi(u)$ show corresponding pattern. Moreover, the inverse relation between porosity and pore pressure changes reveals the effect of pore compacting mechanisms. Differences in $p(u)$ depending on λ are less significant compared to stress and velocity changes, demonstrating the efficiency of porosity changes in controlling the fluid pressure in sealed fault zones. During interseismic compacting periods p is above the background level, whereas coseismic increase in ϕ causes p to drop below the corresponding value of p^{∞} (Hillers & Miller 2006). Note that present changes in p are small compared to those generated by Lockner & Byerlee (1995), Miller *et al.* (1996, 1999), and Fitzenz & Miller (2001) which is due to different pore compacting constitutive laws (Sleep & Blanpied 1992; Sleep 1995). Eq. (8) was found to produce no significant changes in p (Segall & Rice 1995), but within the present framework it has stability controlling properties parametrized by the dilatancy coefficient ε (Fig. 4). Future models that produce a more fertile fluid environment could include fluid sources at depth, or dehydration mechanisms.

Table 1. Overview of the controlling mechanisms and properties ('governing principle') applied in the present study and their influence on specific aspects of the response characteristics. [1]Ruina (1983), [2]Tse & Rice (1986), [3]Rice *et al.* (2001), [4]Rice (1993), [5]Dieterich (1992), [6]Dieterich & Kilgore (1994), [7]Ben-Zion & Rice (1995), [8]Marone (1998), [9]Rubin & Ampuero (2005), [10]Lapusta *et al.* (2000), [11]Bizzarri *et al.* (2001), [12]Tinti *et al.* (2004), [13]Segall & Rice (1995), [14]Taylor & Rice (1998), [15]Hillers & Miller (2006), [16]Ben-Zion & Rice (1995), [17]Ben-Zion (2001), [18]Zöller *et al.* (2005b), [19]Hillers *et al.* (2006a), [20]Hillers *et al.* (2006b).

Governing principle	Controlled response aspect		
Rate-and-state dependence of the friction coefficient	(1) Development of instabilities for $a < b$[1,2,3]	(2) Cyclic seismicity (3) Growth of dynamic instabilities (4) Restrengthening[2,4–10]	(5) Hardening prior to maximum dynamic stress peak[11,12]
Hydromechanics (Compaction and pore pressure evolution)	(1) Stabilizing of $a < b$ areas[13,14]	(2) Generates heterogeneous slip evolution with homogeneous properties[15]	(3) Nucleation in low-p regions (4) Control of event size by pressure state in adjacent areas
Heterogeneity (2-D λ distributions)	Controlling parameter to produce seismicity over several orders of magnitude in discrete[16–18] and continuous models[19,20]		

9 DISCUSSION AND CONCLUSIONS

Extending the analysis of Segall & Rice (1995), our simulations of a 3-D, quasi-dynamic implementation of the conceptual model by Lockner & Byerlee (1995) and Miller *et al.* (1996) demonstrate that instabilities nucleate preferably in low pore pressure regions, and that their extension is controlled by high pressure areas. In particular, effective dilatant mechanisms lead to aseismic, stable response functions of high-p patches, whereas less-effective dilatant hardening allows accelerated slip in these regions but no substantial stress changes. The degree of seismic coupling is controlled by the relative importance of dilatant processes parametrized by the dilatancy coefficient, which is not very well resolved based on laboratory estimates (Segall & Rice 1995; Sleep *et al.* 2000). However, key features of our results remain unaffected by particular choices of ε, as long as large values ($\varepsilon > 3 \times 10^{-4}$) do not stabilize the fault independent of the degree of overpressurization. Hence, the response types depend not only on λ, but on the mechanical interaction of fluid pressure, dilatant effects, the counteracting degree of compressibility, and the (nominal) friction coefficient. Furthermore, the continuous character of the solution—indicated by a sufficient h/h^* ratio—ensures that specific features of the seismic response are not controlled by effects of the spatial discretization, which can not be ruled out in previous discrete studies of hydromechanical interactions (Miller *et al.* 1996, 1999; Fitzenz & Miller 2001). In addition, the rate-and-state formulation does not require an *a priori* defined failure threshold, which has shown to be a powerful method to consistently simulate earthquake cycles with realistic accelerating phases (Dieterich 1992; Rice 1993; Lapusta *et al.* 2000; Rubin & Ampuero 2005).

We observe that instabilities clearly tend to nucleate in regions with low pore pressures, which seems to contradict observations of elevated fluid pressures at hypocentre locations (Zhao *et al.* 1996). This discrepancy between modelling and observational evidence can be assigned to our time-independent treatment of the overpressurization pattern. This computationally necessary simplification does not rule out the possibility that a short-term fluid intrusion triggers seismicity (Miller *et al.* 2004).

Although our model makes major but substantially supported simplifications it allows the efficient investigation of non-uniform slip responses based on likely hydromechanical properties assumed to control the seismic response of sealed and hence weak strike-slip fault zones. However, important processes have not been addressed in the present study that might alter a fluid-infiltrated fault's dynamic slip evolution significantly. Amongst these are fault valve behaviour allowing diffusion processes in the fault and leakage into the host rock (Blanpied *et al.* 1992; Sibson 1994; Sleep 1995; Miller *et al.* 1996), frictional heating (Lachenbruch & Sass 1980; Mase & Smith 1985; Spray 1995; Rice 2006; Bizzarri & Cocco 2006a,b) and slip-induced formation of new cracks (Scholz 1990).

The three main controlling mechanisms and properties that govern certain aspects of the observed response characteristics are summarized in Table 1. It becomes obvious that the effects of each of the single ingredients, rate-and-state friction, hydromechanics, and the role of heterogeneity, are studied in more detail elsewhere. However, the present approach combines these governing principles in a single, consistent 3-D model. Because of previously isolated investigations and applications of the three main mechanisms, we explored their contribution to the response characteristics presented here. In particular, rate-and-state friction allows the efficient investigation of multicycle simulations, hydromechanical processes control the stability of otherwise unstable regions, and imposed heterogeneity leads to seismicity over several orders of magnitude.

It has been shown that regions of near-hydrostatic pore pressure show the largest coseismic slip during unstable slip episodes, compared to regions of near-lithostatic fluid pressure. Corresponding stress evolution reveal that these low-p regions are expected to excite more seismic energy into the crust. Based on simulations presented here we suggest interpreting high-slip regions during earthquakes with relatively dry and hence strong fault sections. Due to the time-independent character of in-fault seals prohibiting pressure equilibration in the fault's core, these strong areas remain spatially immobile in our model. Heterogeneous but static pattern of pore pressure distributions produce non-uniform slip pattern, but the non-uniformity can be related to the governing λ distribution in that low-p regions always respond unstable and high-p regions stable. Thus, the chosen parametrization is sufficient to carefully investigate overpressurization controlled slip pattern with appropriate temporal and spatial resolution, but it lacks the ability to generate highly non-linear slip pattern produced in previous continuous studies (Liu & Rice 2005; Hillers *et al.* 2006a,b).

As has been demonstrated, a relatively large L value and the linear range of physically plausible λ values and the associated variability in the effective nucleation size explain the lack of frequent occurrence of small events. Ben-Zion (1996), Zöller *et al.* (2005b) and Hillers *et al.* (2006b) showed that the range of size scales of the imposed heterogeneity parameter controls the statistics of the associated seismicity pattern. Large ranges of size scales are shown

to result in FMDs that show a Gutenberg-Richter type power-law behaviour and are associated with geometric complexity of fault zones, whereas small ranges of sizes scales lead to a characteristic event type response pattern that correspond to homogeneous fault structures. These studies, and to a lesser degree the present investigation, demonstrate that a linear or log-linear distribution of controlling parameters on a planar model fault is sufficient to generate seismicity over a broad range of scales, in contrast to its often advocated correspondence to fractal parameter distributions (e.g. Scholz & Madelbrot 1989; Turcotte 1997; Dimri 2000; Hergarten 2002; Sornette 2004). FMDs presented here do not reproduce one of the two end-member cases related to fault zone maturity (Wesnousky 1994). However, future use of smaller L values with heterogeneous pore pressure distributions is expected to generate more smaller events due to smaller nucleation sizes. Together with a sufficient range of ε values it is anticipated to lead to a more realistic FMD, indicating that heterogeneous pore pressure states along a fault are related to geometrical complexity.

ACKNOWLEDGMENTS

The manuscript benefited from comments by Massimo Cocco and an anonymous reviewer. The work was sponsored by EC-Project RELIEF (EVG1-CT-2002-00069). This is contribution number 1441 of the Institute of Geophysics, ETH Zurich.

REFERENCES

Andrews, D.J., 2002. A fault constitutive relation accounting for thermal pressurization of pore fluid, *J. Geophy. Res.,* **107**(B12).

Andrews, J., 2006. Thermal pressurization explains enhanced long-period motion in the Chi-Chi earthquake, *Seism. Res. Let.,* **77**(2), 264.

Bak, P. & Tang, C., 1989. Earthquakes as a self-organized critical phenomenon, *J. Geophy. Res.,* **94**(B11), 15 635–15 637.

Bak, P., Tang, C. & Wiesenfeld, K., 1987. Self-organized criticality: an explanation of 1/f noise, *Phys. Rev. Lett.,* **59**(4), 381–384.

Bak, P., Tang, C. & Wiesenfeld, K., 1988. Self-organized criticality, *Phys. Rev. A,* **38**(1), 364–374.

Ben-Zion, Y., 1996. Stress, slip, and earthquakes in models of complex single-fault systems incorporating brittle and creep deformations, *J. Geophys. Res.,* **101**(B3), 5677–5706.

Ben-Zion, Y., 2001. Dynamic rupture in recent models of earthquake faults, *J. Mech. Phys. Solids,* **49,** 2209–2244.

Ben-Zion, Y., 2003. Appendix 2, key formulas in earthquake seismology, in *International Handbook of Earthquake and Engineering Seismology, Part B,* pp. 1857–1875, eds Lee, W.H., Kanamori, H., Jennings, P.C. & Kisslinger, C., Academic Press.

Ben-Zion, Y. & Rice, J.R., 1995. Slip patterns and earthquake populations along different classes of faults in elastic solid, *J. Geophy. Res.,* **100**(B7), 12 959–12 983.

Ben-Zion, Y. & Zhu, L., 2002. Potency-magnitude scaling relations for southern California earthquakes with $1.0 < M_L < 7.0$, *Geophys. J. Int.,* **148,** F1–F5.

Ben-Zion, Y., Eneva, M. & Liu, Y., 2003. Large earthquake cycles and intermittent criticality on heterogeneous faults due to evolving stress and seismicity, *J. Geophy. Res.,* **108**(B6), 1–21.

Bizzarri, A. & Cocco, M., 2006a. A thermal pressurization model for the spontaneous dynamic rupture propagation on a three-dimensional fault: 1. Methodological approach, *J. Geophy. Res.,* **111**(B05303).

Bizzarri, A. & Cocco, M., 2006b. A thermal pressurization model for the spontaneous dynamic rupture propagation on a three-dimensional fault: 2. Traction evolution and dynamic parameters, *J. Geophy. Res.,* **111**(B05304).

Bizzarri, A., Cocco, M., Andrews, D.J. & Boschi, E., 2001. Solving the dynamic rupture problem with different numerical approaches and constitutive laws, *Geophys. J. Int.,* **144,** 656–678.

Blanpied, M.L., Lockner, D.A. & Byerlee, J.D., 1992. An earthquake mechanism based on rapid sealing of faults, *Nature,* **358,** 574–576.

Blanpied, M.L., Marone, C.J., Lockner, D.A., Byerlee, J.D. & King, D.P., 1998. Quantitative measure of the variation in fault rheology due to fluid-rock interactions, *J. Geophy. Res.,* **103**(B5), 9691–9712.

Bosl, W.J. & Nur, A., 2002. Aftershocks and pore fluid diffusion following the 1992 Landers earthquake, *J. Geophy. Res.,* **107**(B12).

Burridge, R. & Knopoff, L., 1967. Model and theoretical seismicity, *Bull. Seism. Soc. Am.,* **57**(3), 341–371.

Caine, J.S., Evans, J.P. & Forster, C.B., 1996. Fault zone architecture and permeability structure, *Geology,* **24**(11), 1025–1028.

Carlson, J.M. & Langer, J.S., 1989a. Properties of earthquakes generated by fault dynamics, *Phys. Rev. Lett.,* **62**(22), 2632–2635.

Carlson, J.M. & Langer, J.S., 1989b. Mechanical model of an earthquake fault, *Phys. Rev. A,* **40**(11), 6470–6468.

Carlson, J.M., Langer, J.S., Shaw, B.E. & Tang, C., 1991. Intrinsic properties of a Burridge-Knopoff model of an earthquake fault, *Phys. Rev. A,* **44**(2), 884–897.

Cox, S.F., 1995. Faulting processes at high fluid pressures: an example of fault valve behavior from the Wattle Gully Fault, Victoria, Australia, *J. Geophy. Res.,* **100**(B7), 12 841–12 859.

Dahmen, K., Ertas, D. & Ben-Zion, Y., 1998. Gutenberg-Richter and characteristic earthquake behavior in simple mean field models of heterogeneous faults, *Phys. Rev. E,* **58**(2), 1494–1501.

Dieterich, J.H., 1992. Earthquake nucleation on faults with rate- and state-dependent strength, *Tectonophysics,* **211,** 115–134.

Dieterich, J.H. & Kilgore, B.D., 1994. Direct observation of frictional contacts: new insights for state-dependent properties, *Pure Appl. Geophys.,* **143**(1/2/3), 283–302.

Dimri, V.P., (ed.) 2000. *Applications of Fractals in Earth Sciences,* A.A. Balkema, Rotterdam.

Fitzenz, D.D. & Miller, S.A., 2001. A forward model for earthquake generation on interacting faults including tectonics, fluids, and stress transfer, *J. Geophy. Res.,* **106**(B11), 26 689–26 706.

Frohlich, C. & Davis, S.D., 1993. Teleseismic b values; or, much ado about 1.0, *J. Geophy. Res.,* **98,** 631–644.

Garagash, D.I. & Rudnicki, J.W., 2003a. Shear heating of a fluid-saturated slip-weakening dilatant fault zone: 1. limiting regimes, *J. Geophy. Res.,* **108**(B2).

Garagash, D.I. & Rudnicki, J.W., 2003b. Shear heating of a fluid-saturated slip-weakening dilatant fault zone: 2. quasi-drained regime, *J. Geophy. Res.,* **108**(B10).

Hairer, E. & Wanner, G., (eds) 1996. *Solving Ordinary Differential Equations II. Stiff and Differential-Algebraic Problems,* 2nd edn, Springer, Berlin.

Hearn, E.H. & Reilinger, R.B. R.E., 2002. Dynamics of izmit earthquake postseismic deformation and loading of the Düzce earthquake hypocenter, *Bull. Seism. Soc. Am.,* **92**(1), 172–193.

Hergarten, S., (ed.) 2002. *Self Organized Criticality in Earth Systems,* 1st edn, Springer, Berlin.

Hickman, S.H., 1991. Stress in the lithosphere and the strength of active faults, *Rev. Geophys.,* pp. 759–775, IUGG Report.

Hillers, G., 2006. On the origin of earthquake complexity in continuum fault models with rate and state friction, Swiss Federal Institute of Technology, *PhD thesis,* Zurich (http://hdl.handle.net/2122/1024).

Hillers, G. & Miller, S.A., 2006. Stability regimes of a dilatant, fluid infiltrated fault plane in a 3-d elastic solid, *J. Geophy. Res.,* **111**(B08304).

Hillers, G., Ben-Zion, Y. & Mai, P.M., 2006a. Seismicity on a fault with rate- and state-dependent friction and spatial variations of the critical slip distance, *J. Geophy. Res.,* **111**(B01403).

Hillers, G., Mai, P.M., Ben-Zion, Y. & Ampuero, J.P., 2006b. Statistical properties of seismicity of fault zones at different evolutionary stages, *Geophys. J. Int.,* revised.

Husen, S., Taylor, R., Smith, R.B. & Healser, H., 2004. Changes in geyser eruption behavior and remotely triggered seismicity in Yellowstone

National Park produced by the 2002 M 7.9 Denali fault earthquake, Alaska, *Geology,* **32**(6), 537–540.

Ito, K. & Matsuzaki, M., 1990. Earthquakes as Self-Organized Critical Phenomena, *J. Geophy. Res.,* **95**(B5), 6853–6860.

Lachenbruch, A.H. & Sass, J.H., 1980. Heat flow and energetics of the San Andreas fault zone, *J. Geophy. Res.,* **85,** 6185–6222.

Langer, J.S., Carlson, J.M., Myers, C.R. & Shaw, B.E., 1996. Slip complexity in dynamic models of earthquake faults, *Proc. Natl. Acad. Sci. USA,* **93,** 3825–3829, Colloquium Paper.

Lapusta, N., Rice, J.R., Ben-Zion, Y. & Zheng, G., 2000. Elastodynamic analysis for slow tectonic loading with spontaneous rupture episodes on faults with rate- and state-dependent friction, *J. Geophy. Res.,* **105**(B10), 23 765–23 789.

Linker, M.F. & Dieterich, J.H., 1992. Effects of Variable Normal Stress on Rock Friction: Observations and Constitutive Equations, *J. Geophy. Res.,* **97**(B4), 4923–4940.

Liu, Y. & Rice, J.R., 2005. Aseismic slip transients emerge spontaneously in three-dimensional rate and state modeling of subduction earthquake sequences, *J. Geophy. Res.,* **110**.

Lockner, D.A. & Byerlee, J.D., 1994. Dilatancy in hydraulically isolated faults and the suppression of instability, *Geophys. Res. Lett.,* **21**(22), 2353–2356.

Lockner, D.A. & Byerlee, J.D., 1995. An earthquake instability model based on faults containing high fluid-pressure compartments, *Pure Appl. Geophys.,* **145**(2/3), 717–745.

Lomnitz-Adler, J., 1993. Automaton models of seismic fracture: constraints imposed by the magnitude-frequency relation, *J. Geophy. Res.,* **98**(B10), 17 745–17 756.

Mai, P.M., 2004. A database of finite-source rupture models (http://www.seismo.ethz.ch/srcmod).

Marone, C., 1998. Laboratory-derived friction laws and their application to seismic faulting, *Annu. Rev. Earth Planet. Sci.,* **26,** 643–696.

Marone, C., Rayleigh, C.B. & Scholz, C.H., 1990. Frictional behavior and constitutive modeling of simulated fault gouge, *J. Geophy. Res.,* **95,** 7007–7025.

Mase, C.W. & Smith, L., 1985. Pore-fluid pressures and fricional heating on a fault surface, *Pure Appl. Geophys.,* pp. 583–607.

Miller, S.A., 2002. Properties of large ruptures and the dynamical influence of fluids on earthquakes and faulting, *J. Geophy. Res.,* **107**(B9).

Miller, S.A., Nur, A. & Olgaard, D.L., 1996. Earthquakes as a coupled shear stress–high pore pressure dynamical system, *Geophys. Res. Lett.,* **23**(2), 197–200.

Miller, S.A., Ben-Zion, Y. & Burg, J.-P., 1999. A three-dimensional fluid-controlled earthquake model: behavior and implications, *J. Geophy. Res.,* **104**(B5), 10 621–10 638.

Miller, S.A., Collettini, C., Chiaraluce, L., Cocco, M., Barchi, M. & Kaus, J.P., 2004. Aftershocks driven by a high-pressure CO_2 source at depth, *Nature,* **427,** 724–727.

Moore, J.C., Lockner, D.A. & Byerlee, J.D., 1994. Reduction of permeability in granite at elevated temperatures, *Science,* **265,** 1558–1561.

Nur, A. & Booker, J.R., 1972. Aftershocks caused by pore fluid flow?, *Science,* **175,** 885–887.

Nur, A. & Walder, J., 1992. Hydraulic pulses in the Earth's crust, in *Fault Mechanics and Transport Properties in Rocks,* pp. 459–473, eds Evans, B. & Wong, T.-F., Academic Press, San Diego, CA.

Ohnaka, M., 1996. Nonuniformity of the constitutive law parameters for shear rupture and quasistatic nucleationto dynamic rupture: a physical model of earthquake generation processes, *Proc. Natl. Acad. Sci. USA,* **93,** 3795–3802, Colloquium Paper.

Ohnaka, M., 2003. A constitutive scaling law and a unified comprehension for frictional slip failure, shear fracture of intact rock, and earthquake rupture, *J. Geophy. Res.,* **108**(B2).

Ohnaka, M. & Shen, L.-F., 1999. Scaling of the shear rupture process from nucleation to dynamic propagation: Implications of geometric irregularity of the rupture surfaces, *J. Geophy. Res.,* **104**(B1), 817–844.

Piatanesi, A., Tinti, E., Cocco, M. & Fukuyama, E., 2004. The dependence of traction evolution on the earthquake source time function adopted in kinematic rupture models, *Geophys. Res. Lett.,* **31**.

Piombo, A., Martinelli, G. & Dragoni, M., 2005. Post-seismic fluid flow and Coulomb stress changes in a poroelastic medium, *Geophys. J. Int.,* **162,** 507–515.

Reilinger, R.E. et al., 2000. Coseismic and postseismic fault slip for the 17 August 1999, $M = 7.5$, Izmit, Turkey earthquake, *Science,* **289,** 1519–1523.

Rice, J.R., 1992. Fault Stress States, Pore Pressure Distributions, and the Weakness of the San Andreas Fault, in *Fault Mechanics and Transport Properties in Rocks,* pp. 475–503, eds Evans, B. & Wong, T.-F., Academic Press, San Diego, CA.

Rice, J.R., 1993. Spatio-temporal complexity of slip on a fault, *J. Geophy. Res.,* **98**(B6), 9885–9907.

Rice, J.R., 2006. Heating and weakening of faults during earthquake slip, *J. Geophy. Res.,* **111**(B05311).

Rice, J.R. & Ben-Zion, Y., 1996. Slip complexity in earthquake fault models, *Proc. Natl. Acad. Sci. USA,* **93,** 3811–3818, Colloquium Paper.

Rice, J.R., Lapusta, N. & Ranjith, K., 2001. Rate and state dependent friction and the stability of sliding between elastically deformable solids, *J. Mech. Phys. Solids,* **49,** 1865–1898.

Rubin, A.M. & Ampuero, J.-P., 2005. Earthquake nucleation on (aging) rate and state faults, *J. Geophy. Res.,* **110**(B11312).

Ruina, A., 1983. Slip instability and state variable friction laws, *J. Geophy. Res.,* **88**(B12), 10 359–10 370.

Scholz, C.H., (ed.) 1990. *The Mechanics of Earthquakes and Faulting,* 1st edn, Cambridge University Press, Cambridge.

Scholz, C.H. & Madelbrot, B.B., (eds) 1989. *Fractals in Geophysics; Reprint from PAGEOPH, Vol. 131 (1989), no. 1/2,* Birkhäuser, Basel.

Segall, P., 1996. Earthquakes: slow down for safety, *Nature, News and Views,* **383,** 21–22.

Segall, P. & Rice, J.R., 1995. Dilatancy, compaction, and slip instability of a fluid-infiltrated fault, *J. Geophy. Res.,* **100**(B11), 22 155–22 171.

Sibson, R.H., 1992. Implications of fault-valve behavior for rupture nucleation and recurrence, *Tectonophysics,* **211,** 283–293.

Sibson, R.H., 1994. Crustal stress, faulting and fluid flow, in *Geofluids: Origin, Migration and Evolution of Fluids in Sedimentary Basins,* pp. 69–84, ed. Parnell, J., Geological Society Special Publication No. 78.

Sleep, N.H., 1995. Ductile creep, compaction, and rate and state dependent friction within major fault zones, *J. Geophy. Res.,* **100**(B7), 13 065–13 080.

Sleep, N.H. & Blanpied, M.L., 1992. Creep, compaction and the weak rheology of major faults, *Nature,* **359,** 687–692.

Sleep, N.H., Richardson, E. & Marone, C., 2000. Physics of friction and strain rate localization in synthetic fault gouge, *J. Geophy. Res.,* **105**(B11), 28 875–25 890.

Sornette, D., (ed.) 2004. *Critical Phenomena in Natural Sciences,* 2nd edn, Springer, Berlin.

Spray, J.G., 1995. Pseudotachylyte controversy: fact or fiction?, *Geology,* pp. 1119–1122.

Stuart, W.D. & Tullis, T.E., 1995. Fault model for preseismic deformation at Parkfield, California, *J. Geophy. Res.,* **100,** 24 079–24 099.

Taylor, M.A.J. & Rice, J.R., 1998. Dilatant stabilization of subduction earthquake rupture into the shallow thrust interface, *Eos Trans. AGU,* **79**(45), F631.

Tinti, E., Bizzarri, A., Piatanesi, A. & Cocco, M., 2004. Estimates of slip weakening distance for different dynamic rupture models, *Geophys. Res. Lett.,* **31**.

Tse, S.T. & Rice, J.R., 1986. Crustal earthquake instability in relation to the depth variation of frictional slip properties, *J. Geophy. Res.,* **91**(B9), 9452–9472.

Turcotte, D.L., (ed.) 1997. *Fractals and Chaos in Geology and Geophysics,* 2nd edn, Cambridge Univ. Press, New York.

Waite, G.P. & Smith, R.B., 2002. Seismic evidence for fluid migration accompanying subsidence of the Yellowstone caldera, *J. Geophy. Res.,* **107** (B9).

Walder, J. & Nur, A., 1984. Porosity reduction and pore pressure development, *J. Geophy. Res.,* **89,** 11 539–11 548.

Wesnousky, S.G., 1994. The Gutenberg-Richter or characteristic earthquake distribution, which is It?, *Bull. Seism. Soc. Am.,* **84**(6), 1940–1959.

Wibberly, C.A.J. & Shimamoto, T., 2003. Internal structure and permeability of major strike-slip fault zones: the Median Tectonic Line in Mie Prefecture, Southwest Japan, *J. Struct. Geol.,* **25,** 59–78.

Zhang, S. & Tullis, T.E., 1998. The effect of fault slip on permeability and permeability anisotropy in quartz gouge, *Tectonophysics,* **295,** 41–52.

Zhang, S., Tullis, T.E. & Scruggs, V.J., 1999. Permeability anisotropy and pressure dependency of permeability in experimentally sheared gouge materials, *J. Struct. Geol.,* **21,** 795–806.

Zhang, S., Tullis, T.E. & Scruggs, V.J., 2001. Implications of permeability and its anisotropy in a mica gouge for pore pressure in fault zones, *Tectonophysics,* **335,** 37–50.

Zhao, D., Kanamori, D., Negishi, H. & Wiens, D., 1996. Tomography of the source area of the 1995 Kobe earthquake: evidence for fluids at the hypocenter?, *Science,* **274**(5294), 1891–1894.

Zöller, G., Hainzl, S., Hohlschneider, M. & Ben-Zion, Y., 2005a. Aftershocks resulting from creeping sections in a heterogeneous fault, *Geophys. Res. Lett.,* **32**.

Zöller, G., Hohlschneider, M. & Ben-Zion, Y., 2005b. The role of heterogeneities as a tuning parameter of earthquake dynamics, *Pure Appl. Geophys.,* **162,** 1077–1111.